

# Mixture of Group Experts for Learning Invariant Representations

Lei Kang  
Beijing Normal University  
Beijing, China  
leikang@mail.bnu.edu.cn

Mi Tian  
TAL Education Group  
Beijing, China  
tianmi@tal.com

Jia Li  
Beijing Normal University  
Beijing, China  
jiali@bnu.edu.cn

Hua Huang  
Beijing Normal University  
Beijing, China  
huahuang@bnu.edu.cn

## Abstract

Sparsely activated Mixture-of-Experts (MoE) models effectively increase the number of parameters while maintaining consistent computational costs per token. However, vanilla MoE models often suffer from limited diversity and specialization among experts, constraining their performance and scalability, especially as the number of experts increases. In this paper, we present a novel perspective on vanilla MoE with top- $k$  routing inspired by sparse representation. This allows us to bridge established theoretical insights from sparse representation into MoE models. Building on this foundation, we propose a group sparse regularization approach for the input of top- $k$  routing, termed Mixture of Group Experts (MoGE). MoGE indirectly regularizes experts by imposing structural constraints on the routing inputs, while preserving the original MoE architecture. Furthermore, we organize the routing input into a 2D topographic map, spatially grouping neighboring elements. This structure enables MoGE to capture representations invariant to minor transformations, thereby significantly enhancing expert diversity and specialization. Comprehensive evaluations across various Transformer models for image classification and language modeling tasks demonstrate that MoGE substantially outperforms its MoE counterpart, with minimal additional memory and computation overhead. Our approach provides a simple yet effective solution to scale the number of experts and reduce redundancy among them. The source code is included in the supplementary material and will be publicly released.

## Keywords

Mixture-of-Experts, Group Sparsity, Invariant Representations

## 1 Introduction

Transformer models [42] have consistently demonstrated performance improvements as their parameter counts increase [21]. However, the growth in model size comes with significant computational costs, making further scaling increasingly challenging. Sparsely activated Mixture-of-Experts (MoE) [38] offers a promising solution by utilizing a sparse architecture that activates only a subset of parameters during both training and inference. As shown in Fig. 1 (a), an MoE layer comprises multiple experts, activating only a few experts for each input token. A gating network is trained to route each token to the most suitable experts. This conditional computation enables MoE models to significantly increase their capacity without a rise in computation overhead. By integrating

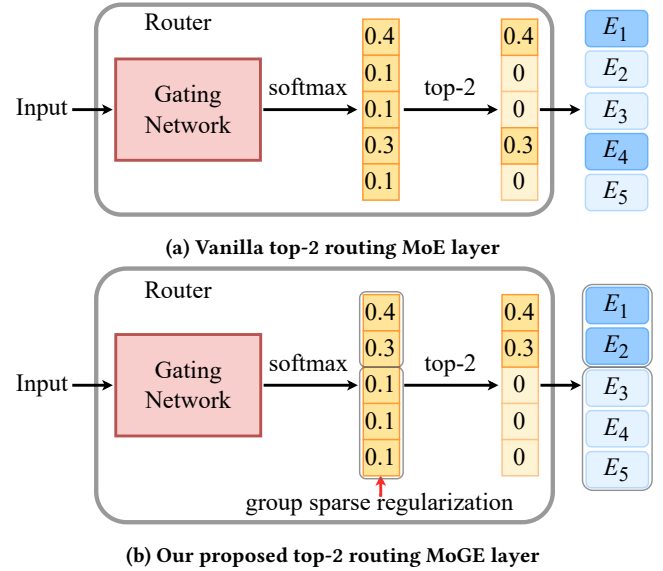


**Figure 1: A high-level comparison between the vanilla MoE layer and the proposed MoGE layer. (a) illustrates the vanilla MoE layer with the top-2 routing, while (b) demonstrates the application of group sparse regularization in MoGE. It is important to note that the using of group sparse regularization does not alter the MoE architecture. In the vanilla MoE, each element in the input of top-2 routing is independent and considered part of a single group. In contrast, MoGE introduces a grouping mechanism that partitions the input of top-2 routing into two groups: the first two elements in one group and the remaining three elements in the other. This grouping effect naturally extends to the subsequent organization  $\{E_1, \dots, E_5\}$ , resulting in their corresponding organization into same groups.**

MoE layers into Transformer models, researchers have successfully scaled large foundation models to impressive sizes, achieving outstanding performance in tasks such as image classification [15, 36] and language modeling [3, 40].

Despite their advantages, MoE models face a critical challenge: the lack of diversity and specialization among experts [8, 35, 39, 44, 54]. In an MoE layer, a gating network determines token-to-expert mappings, ideally routing similar or relevant tokens to the same

group of experts. However, the vanilla MoE layer often produces redundant experts that fail to achieve sufficient diversity and specialization, thereby undermining the performance of MoE models. Promoting diversity and specialization among experts remains a significant challenge for MoE models, especially as the number of experts scales.

**Contributions:** In this paper, we reinterpret the combination of the most popular top- $k$  routing and experts as a form of sparse representation. Building on this perspective, we propose a novel regularization technique that is applied to the routing inputs, rather than directly constraining the experts themselves, to promote greater diversity and specialization. Our approach does not require modifications to the MoE architecture and can be directly applied to any MoE model. The main contributions are highlighted below.

Firstly, we propose investigating MoE employing top- $k$  routing from the perspective of sparse representation. Sparse representation aims to find the sparse code that effectively approximates the input when multiplied with the dictionary [4, 41]. For the MoE with top- $k$  routing, the routing output can be viewed as the sparse code, while the output of each expert corresponds to a column in the dictionary. This perspective enables the application of the rich theoretical results of sparse representation to MoE.

Secondly, we propose introducing group sparse regularization to the inputs of top- $k$  routing to indirectly impose structural constraints on experts. Group sparsity assumes that the input elements of top- $k$  routing are organized into predefined groups, where all elements within a group tend to be either all zeros or all nonzeros [6, 53]. These groups are typically formed based on an arbitrary partition, informed by prior knowledge specific to the task. As illustrated in Fig. 1 (b), we refer to the application of group sparse regularization in MoE as the Mixture of Group Experts (MoGE). Inspired by previous works [16, 17, 22], we further organize the routing input into a 2D matrix, forming a topographic map where neighboring elements are grouped together to activate similar experts. This topographically organized input enables MoGE to extract locally invariant representations, encouraging diversity and specialization among experts.

Finally, we evaluate our MoGE across various image classification and language modeling tasks. Consistently, our MoGE demonstrates superior performance compared to its MoE counterpart, with only a negligible increase in memory consumption and computational cost. Additionally, our MoGE effectively promotes diversity and specialization among experts through an easily implementable approach, enabling the training of a greater number of experts and larger  $k$  values in top- $k$  routing.

## 2 Related Work

### 2.1 Mixture-of-Experts

Mixture-of-Experts (MoE) was first introduced in the early 1990s [18, 20]. Later, Shazeer et al. [38] proposed integrating an MoE layer between LSTM layers, leading to remarkable advancements in machine translation. This idea was further extended by incorporating the MoE layer into the Transformer architecture, replacing traditional feedforward layers. For example, GShard [27] refines the top-2 routing strategy, significantly boosting machine translation performance. Switch Transformer [7] simplifies the gating

mechanism by selecting only the top-1 expert per token, achieving superior scalability. More recently, PEER [11] introduces an expansion of the expert count in MoE to one million, showcasing its potential in pushing the boundaries of MoE models. Commercial-scale language models have also adopted MoE architectures, with notable examples including Mixtral-8x7B [19], Qwen2.5 [51], and DeepSeek-V3 [28].

### 2.2 Promoting Expert Diversity

Researchers have developed a variety of strategies to construct diverse experts, drawing inspiration from ensemble learning [47]. Some methods focus on leveraging different initialization techniques. For instance, MMoE [33] achieves expert diversity by introducing varying degrees of randomness into both the training data and model initialization processes. Similarly, MoE Jetpack [55] employs diverse dense checkpoints to initialize different experts, while Drop-Upcycling [35] takes an alternative approach by using pre-trained dense models for initialization, followed by a strategic re-initialization of specific weight components to enhance diversity. Other approaches aim to diversify experts by training them on distinct datasets. For example, MoCLE [9] clusters the training data into multiple groups using a pre-trained clustering model and learns to activate specific LoRA experts at each layer based on the data cluster. Structural variations have also proven effective for promoting expert diversity. MLoRE [52] utilizes low-rank experts with varying ranks, while HMoE [44] and MoDSE [39] achieve diversity by incorporating experts of different sizes. Advances in token-to-expert mapping represent another avenue for innovation. MMoEEx [1], for instance, employs exclusion and exclusivity mechanisms to induce diversity among experts. Meanwhile, Zhou et al. [54] propose an alternative approach through expert-choice routing, wherein tokens may be processed by a variable number of experts rather than adhering to conventional token-choice routing mechanisms. Additionally, shared experts have garnered attention in recent works [10, 28], demonstrating significant adaptability and efficiency by remaining universally activated. Regularization techniques further enhance expert diversity. For example, MOORE [12] combines the Gram-Schmidt process with reinforcement learning to orthogonalize expert-generated representations, promoting decorrelation among experts. Similarly, OMoE [8] applies an orthogonalization technique during fine-tuning. Meanwhile, MoELoRA [32] employs a contrastive learning framework, treating outputs from the same expert as positive samples and those from different experts as negative ones.

## 3 Methodology

In this section, we begin by introducing the vanilla MoE, followed by an analysis of MoE from the perspective of sparse representation. We then provide a comprehensive explanation of the implementation process and underlying mechanism of our proposed MoGE. Finally, we investigate how MoGE effectively learns invariant representations.

### 3.1 Vanilla MoE

To recap the core concepts behind our MoGE, we focus specifically on the sparsely activated MoE layer and the top- $k$  routing. Existing

MoE models are typically derived from dense Transformer models by replacing certain feedforward layers with MoE layers [7, 19, 36]. As illustrated in Fig. 1 (a), an MoE layer generally consists of a set of experts  $\{E_1(\cdot), \dots, E_n(\cdot)\}$  and a router that directs input tokens to the most relevant experts. Here,  $n$  denotes the total number of experts, and  $E_i(\cdot) \in \mathbb{R}^m$  for  $i = 1, \dots, n$ .

The router leverages the top- $k$  routing mechanism to reduce computation overhead by selectively activating only the top- $k$  experts deemed most relevant to each input token. It typically includes a gating network  $G(\cdot)$ , a softmax function, and a top- $k$  function. For any input token  $x$ , the routing decision is computed as follows:

$$z = \text{softmax}(G(x)), \quad (1)$$

where  $z \in \mathbb{R}^n$ . Subsequently, sparsely activated weights are computed using:

$$w = \text{TopK}(z, k), \quad (2)$$

where the top- $k$  function,  $\text{TopK}(\cdot, \cdot)$ , is defined as:

$$\text{TopK}(v, k) = \begin{cases} v_i, & \text{if } v_i \text{ is among the top-}k \text{ elements of } v; \\ 0, & \text{otherwise.} \end{cases} \quad (3)$$

The final output  $y \in \mathbb{R}^m$  of the MoE layer is computed as a linear combination of the outputs from the selected experts weighted by the sparsely activated weights:

$$y = \sum_{i \in \mathcal{I}} w_i E_i(x), \quad (4)$$

where  $\mathcal{I}$  denotes the set of top- $k$  indices derived from  $z$ .

For simplicity, we omit considerations of noise, load balancing loss, and any sequence dependencies between the softmax and the top- $k$  functions. In our experiments, we follow the default settings for each MoE model outlined in its original paper.

### 3.2 Sparse Representation for MoE

Given an overcomplete dictionary  $\mathcal{D} \in \mathbb{R}^{m \times n}$  ( $m < n$ ), sparse representation [4, 41, 48] expresses an input signal  $y \in \mathbb{R}^m$  as the product of the dictionary  $\mathcal{D}$  and a sparse code  $w \in \mathbb{R}^n$ . Namely,  $y$  is represented as a linear combination of the columns of the dictionary  $\mathcal{D}$ , weighted by elements in the sparse code  $w$ . When the number of nonzero elements in  $w$  is constrained to be no greater than  $k$ , the sparse representation problem can be formulated as:

$$\min_w \frac{1}{2} \|y - \mathcal{D}w\|_2^2, \quad \text{s.t. } \|w\|_0 \leq k, \quad (5)$$

where  $\|w\|_0$  denotes the count of nonzero elements in  $w$ .

By treating  $E_i(x)$  as the  $i$ -th column of the dictionary  $\mathcal{D}$ , Eqs. (2) and (4) can be interpreted as the solution to problem (5). Consequently, the MoE layer utilizing top- $k$  routing can be viewed as addressing a sparse representation problem. Sparse representation, having been developed over the past two decades, offers a wealth of validated theoretical foundations that can be effectively leveraged in the design of MoE models.

In this paper, we adopt the simplest approach by promoting the diversity and specialization of experts through the application of regularization to the sparse code  $w$ . However, due to the limited number of experts, the  $k$  value is usually small, with  $k = 1$  and  $k = 2$  being the most commonly used. The high sparsity of nonzero elements in  $w$  diminishes the effectiveness of regularization. To

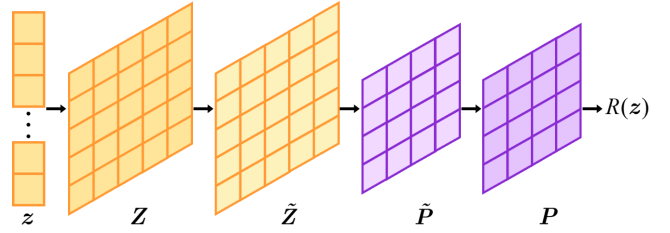


**Figure 2: Illustrating the computation process of our group sparse regularization.**

address this, we propose applying regularization to  $z$  in (1), which serves as the input to the top- $k$  function.

### 3.3 Mixture of Group Experts

Adding structural constraints to sparse codes has been demonstrated as an effective strategy. In the original problem presented in (5), any column of the dictionary can be selected freely. However, in the structured sparse model [6, 53], instead of selecting individual columns, groups of columns are selected collectively. These groups can overlap and vary in size, with the goal of representing  $y$  such that the code  $w$  remains sparse while adhering to the imposed structure. Typically, these groups are defined based on prior knowledge relevant to the task. We refer to the incorporation of group sparse regularization in MoE as the Mixture of Group Experts (MoGE) (see Fig. 1 (b)).

Designing a structural constraint for sparse codes that performs effectively across diverse tasks is a significant challenge. A widely adopted general structural constraint is local invariance, which ensures that the output remains consistent when the input undergoes minor transformations. For instance, in image classification tasks, small perturbations of the input images such as translations, rotations, scalings, or degradations should not drastically affect the extracted features. In the context of MoGE, we strive for the corresponding representation  $z$  to exhibit invariance under small changes to the input token  $x$ . This property ensures that the selection of experts remains consistent, thereby mapping similar tokens to similar experts. Since these experts process analogous tokens as input, they can enhance diversity and specialization.

Building upon the foundational studies of the visual cortex [16, 17, 22], we propose a topographically organized regularization for  $z$  aimed at facilitating the learning of invariant representations. Specifically, our approach employs group sparse regularization, structuring  $z$  into a 2D matrix to form a topographic map. This arrangement encourages neighboring elements to activate similar experts, thereby preserving local invariance. Moreover, this design enhances both the consistency and interpretability of expert selection, offering a robust framework for structured representation learning.

We first introduce the computation process of our group sparse regularization for  $z$  and then provide an analysis of the underlying reasoning. The computation process is illustrated in Fig. 2. Given a vector  $z \in \mathbb{R}^n$ , we begin by reshaping it into an approximately square matrix  $Z \in \mathbb{R}^{r \times c}$ , where  $n = r \times c$  and  $r$  is chosen to be as close to  $c$  as possible. Next, we compute the elementwise square

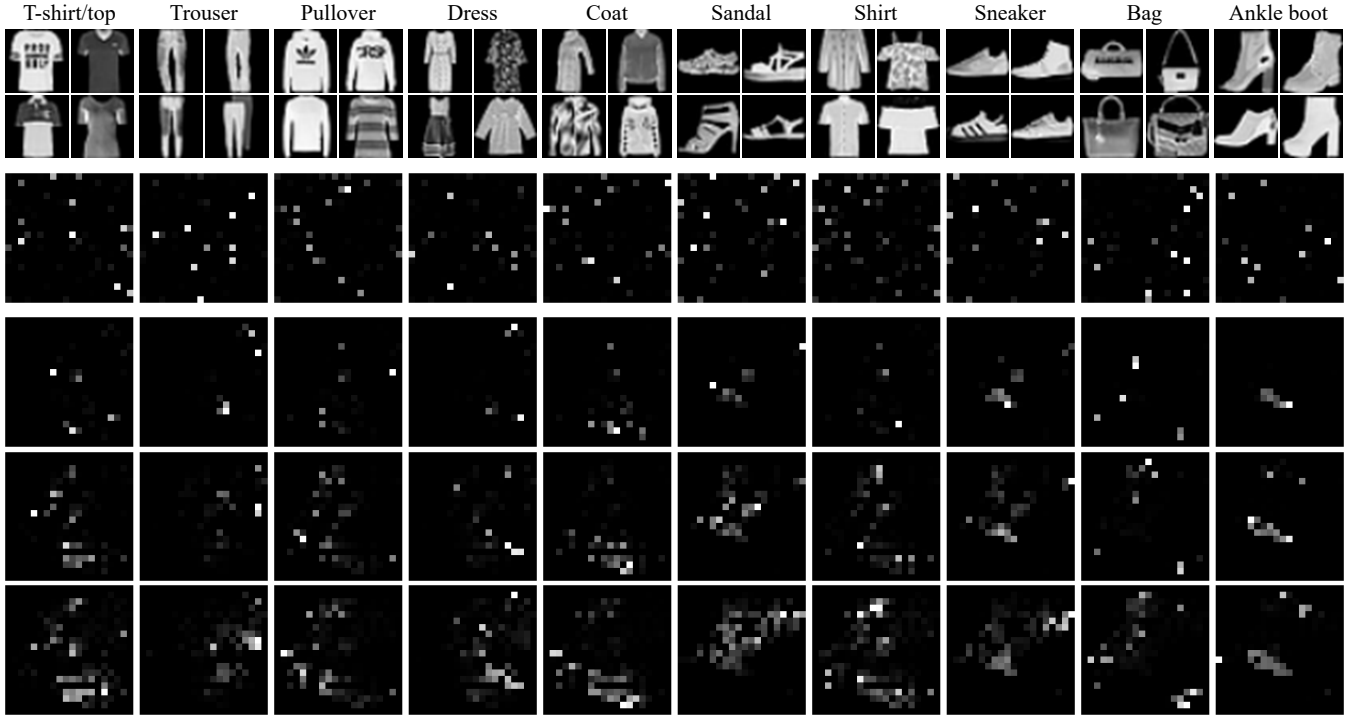


Figure 3: The average inputs of top-1 routing in 2D (denoted as  $Z$  in Algorithm 1) of MoE and MoGE for each category in the Fashion-MNIST test set. The first row corresponds to the ten categories in the Fashion-MNIST dataset. The second row shows the average of  $Z$  for MoE across each category at the 150th epoch. The subsequent three rows display the average of  $Z$  for MoGE across each category at the 50th, 100th, and 150th epochs, respectively. We can see that the average elements of  $Z$  in MoGE demonstrate a clear aggregation effect throughout the training process. In contrast, such an aggregation effect is absent in MoE.

---

**Algorithm 1** Computing our group sparse regularization.

---

**Input:** input of top- $k$  routing  $z \in \mathbb{R}^n$ , size  $h$  and standard deviation  $\sigma$  of Gaussian lowpass filter.

**Output:** group sparse regularization  $R(z) \in \mathbb{R}$ .

- 1: Reshape  $z \in \mathbb{R}^n$  into an approximate square matrix  $Z \in \mathbb{R}^{r \times c}$  such that  $n = r \times c$  and  $r$  is close to  $c$
  - 2: Compute  $\tilde{Z} = Z \odot Z$
  - 3: Generate Gaussian filter  $F_\sigma \in \mathbb{R}^{h \times h}$
  - 4: Compute the 2D convolution  $\tilde{P} = F_\sigma * \tilde{Z}$
  - 5: Compute  $P = \sqrt{\tilde{P}}$
  - 6: Compute group sparse regularization  $R(z) = \sum_i \sum_j P_{ij}$
- 

of  $Z$  to obtain  $\tilde{Z}$ , i.e.,  $\tilde{Z} = Z \odot Z$ , where  $\odot$  denotes the element-wise product. Subsequently, we generate a rotationally symmetric Gaussian lowpass filter  $F_\sigma$  of size  $h \times h$  with a standard deviation  $\sigma$ . We then convolve  $\tilde{Z}$  with the Gaussian filter  $F_\sigma$  to produce  $\tilde{P}$ , i.e.,  $\tilde{P} = F_\sigma * \tilde{Z}$ , where  $*$  denotes the 2D convolution. Finally, we compute the square root of each element in  $\tilde{P}$  to obtain  $P$ . The group sparse regularization  $R(z)$  is defined as the sum of all elements in  $P$ . We summarize the entire computation process of our group sparse regularization in Algorithm 1.

To illustrate the mechanism of our group sparse regularization, we first introduce the general form of  $l_{p,q}$  group sparse regularization [13]. Consider the group structure of  $z$ , represented as  $\{z_{\mathcal{G}_1}, \dots, z_{\mathcal{G}_s}\}$ . The  $l_{p,q}$  group sparse regularization of  $z$  is defined as follows:

$$\|z\|_{p,q} = \left( \sum_{i=1}^s \|z_{\mathcal{G}_i}\|_p^q \right)^{1/q}, \quad (6)$$

where  $s$  denotes the number of groups,  $p \geq 1$ ,  $0 \leq q \leq 1$ , and  $\|\cdot\|_p$  denotes the  $l_p$ -norm for  $p > 0$ , defined as  $\|z\|_p = (\sum_i |z_i|^p)^{1/p}$ . The  $l_{p,q}$  group sparse regularization encourages all elements within each group to be either entirely zero or entirely nonzero. A widely used special case is the  $l_{2,1}$  regularization, defined as:

$$\|z\|_{2,1} = \sum_{i=1}^s \|z_{\mathcal{G}_i}\|_2. \quad (7)$$

In Algorithm 1, when we employ an average filter of size  $h \times h$  instead of a Gaussian filter, it is clear that our group sparse regularization corresponds to  $l_{2,1}$  regularization, where all elements within each local neighborhood of size  $h \times h$  are vectorized and assigned to a group and spatially adjacent groups are overlapping. This design enables our group sparse regularization to cluster neighboring elements in  $Z$ , thereby activating similar experts. We simply set  $p = 2$  and  $q = 1$  in our current approach. Other configurations satisfying

**Table 1: Comparison of the average image Euclidean distances in  $Z$  between the original images from the Fashion-MNIST test set and their corresponding variations under different transformations. A smaller value indicates a higher degree of invariance in  $Z$  to the respective transformation.**

Type	Rotation			Scaling			Translation			Shear		
	5	10	15	0.5	0.8	1.1	(0, 0.1)	(0.1, 0)	(0.1, 0.1)	5	10	15
MoE	0.0778	0.1301	0.1670	0.2359	0.2268	0.1466	0.1181	0.1218	0.1759	0.0345	0.0671	0.0980
MoGE	<b>0.0473</b>	<b>0.0811</b>	<b>0.1067</b>	<b>0.1948</b>	<b>0.1680</b>	<b>0.1147</b>	<b>0.0786</b>	<b>0.0809</b>	<b>0.1206</b>	<b>0.0209</b>	<b>0.0396</b>	<b>0.0576</b>

$p \geq 1$  and  $0 \leq q \leq 1$  are also applicable. A thorough investigation of the effects of varying  $p$  and  $q$  is deferred to future work.

We use a Gaussian filter instead of an average filter for the following two key reasons. First, unlike the average filter, the Gaussian filter preserves the 2D structural information within the group by incorporating the distance from the center into its calculations. Second, the Gaussian filter provides the flexibility to adjust the standard deviation  $\sigma$ . A larger  $\sigma$  facilitates sufficient competition within the group, while a smaller  $\sigma$  encourages aggregation. In practice, the standard deviation  $\sigma$  is not fixed and can follow a dynamic scheduling strategy, enabling it to adapt throughout the training process. We aim to promote sufficient competition among group elements during the early stages of training, while encouraging them to become more concentrated as training progresses. To achieve this, we employ the following pow function scheduling:

$$\sigma_t = \sigma_0 - (\sigma_0 - \sigma_{\min}) \left(\frac{t}{T}\right)^\gamma, \quad (8)$$

where  $\sigma_0 > 0$  and  $\sigma_{\min} > 0$  are constants satisfying  $\sigma_0 \geq \sigma_{\min}$ .  $\gamma \geq 0$ ,  $t$  represents the current iteration number, and  $T$  is the total number of iterations. The curves of  $\sigma$  with varying  $\gamma$  over iterations are illustrated in Appendix A. Finding the optimal scheduler for  $\sigma$  is a challenging task. This complexity arises not only from the intricate interplay between learning rate, batch size, number of experts  $n$ , the  $k$  value, and other hyperparameters but also from the prohibitively high cost of conducting a hyperparameter search for MoE models with massive parameters [2]. We will explore optimal scheduler for  $\sigma$  in the future.

We incorporate the proposed group sparse regularization  $R(z)$  into the vanilla MoE with its original loss function  $\mathcal{L}$ , resulting in the following loss function for MoGE:

$$\mathcal{L} + \lambda R(z), \quad (9)$$

where  $\lambda > 0$  balances the original loss function and the regularization. Our group sparse regularization requires computing a 2D convolution with a Gaussian lowpass filter (see Algorithm 1). In practice, we empirically use valid convolution to avoid padding operations on  $\tilde{Z}$  (see Fig. 2). Additionally, we need to predefine the filter size  $h$  and the standard deviation  $\sigma$ . In subsection 4.4, we will conduct ablation experiments to analyze these aspects.

### 3.4 Investigating Invariant Representations

We explore how MoGE learns invariant representations by employing a simplified model with a single MoE layer for image classification on the Fashion-MNIST dataset [49]. The model consists of 400 homogeneous experts with top-1 routing, where each image is treated as a token. Each expert is a two-layer feedforward network,

featuring 784 neurons in both the input and output layers, and 64 neurons in the hidden layer. The output of the MoE layer is fed directly into a single-layer feedforward classifier for categorization into 10 classes.

We train MoE and MoGE models from scratch for 150 epochs, setting  $h = 3$ ,  $\sigma = 2$ , and  $\lambda = 4e-3$  for MoGE. The top-1 test accuracies achieved by MoE and MoGE are 41.70% and 44.74%, respectively. Due to the large number of experts and the relatively small size of the training set, these test accuracies are not particularly high. However, our primary focus here is on the relative performance of the two models. Fig. 3 illustrates the average  $Z$  values in Algorithm 1 for both MoE and MoGE across each category in the Fashion-MNIST test set. Notably, the average elements of  $Z$  in MoGE exhibit a clear aggregation effect throughout the training process. In contrast, this aggregation effect is not observed in MoE. This indicates that the experts activated for each category in MoGE exhibit spatial similarity, which helps enhance the diversity and specialization of the experts.

To validate that MoGE effectively learns invariant representations, we apply various transformations to the images in the Fashion-MNIST test set and evaluate the image Euclidean distances (IMED) [45] in  $Z$  between the original and the transformed images. Unlike the standard Euclidean distance, which assumes spatial independence of pixels and may produce counterintuitive results (e.g., assigning smaller distances to perceptually significant distortions), IMED takes into account the spatial correlations between pixels. This characteristic makes IMED a widely adopted metric for comparing 2D images. As shown in Table 1, we use the default function `RandomAffine` in PyTorch to implement four transformations: rotation, scaling, translation, and shear. The rotation transformation rotates input images by angles of 5, 10, and 15 degrees. The scaling transformation applies scale factors of 0.5, 0.8, and 1.1. The translation transformation shifts images horizontally and vertically by (0, 0.1), (0.1, 0), and (0.1, 0.1), relative to the image size. The shear transformation utilizes shear angles of 5, 10, and 15 degrees. The results reported in Table 1 demonstrate that following these transformations, the average IMED values in  $Z$  for MoGE are consistently smaller than those for MoE. This highlights the significant advantage of MoGE in learning more invariant representations.

## 4 Experiments

In this section, we first evaluate the superiority of MoGE on image classification and language modeling tasks. Subsequently, we test the scalability and efficiency of MoGE, followed by ablation studies on the Gaussian lowpass filter.

**Table 2: Comparison of the dense, MoE, and our MoGE models for training from scratch and fine-tuning in image classification.**

Dataset	Model	Resolution	Acc@1	Acc@5	$n$	$k$	#Params	#Params <sub>act</sub>
CIFAR-100	ViT-S/4 [5]	$32 \times 32$	74.31	91.34	-	-	25.3M	25.3M
	V-MoE-S/4 [36]		74.03	91.49	32	1	155.5M	25.4M
	V-MoGE-S/4		<b>74.67</b>	<b>91.55</b>	32	1	155.5M	25.4M
	SwinV2-T/4 [29]	$32 \times 32$	76.62	92.09	-	-	27.7M	27.7M
	SwinV2-MoE-T/4 [15]		77.35	92.41	32	1	284.0M	27.7M
	SwinV2-MoGE-T/4		<b>77.75</b>	<b>92.61</b>	32	1	284.0M	27.7M
Tiny-ImageNet	ViT-S/8 [5]	$64 \times 64$	55.11	76.25	-	-	25.5M	25.5M
	V-MoE-S/8 [36]		55.38	76.66	32	1	155.7M	25.5M
	V-MoGE-S/8		<b>56.15</b>	<b>77.24</b>	32	1	155.7M	25.5M
	SwinV2-T/7 [29]	$64 \times 64$	58.42	77.72	-	-	27.7M	27.7M
	SwinV2-MoE-T/7 [15]		59.01	78.97	32	1	284.1M	27.8M
	SwinV2-MoGE-T/7		<b>60.19</b>	<b>79.50</b>	32	1	284.1M	27.8M
ImageNet-1K	ViT-S/16 [5]	$224 \times 224$	<b>77.81</b>	<b>93.78</b>	-	-	26.2M	26.2M
	V-MoE-S/16 [36]		76.95	92.95	32	1	156.4M	26.3M
	V-MoGE-S/16		77.24	93.18	32	1	156.4M	26.3M
	SwinV2-T/12 [29]	$192 \times 192$	<b>80.43</b>	<b>95.30</b>	-	-	28.3M	28.3M
	SwinV2-MoE-T/12 [15]		79.14	94.00	32	1	211.4M	28.4M
	SwinV2-MoGE-T/12		79.97	94.94	32	1	211.4M	28.4M
ImageNet-1K (fine-tuning)	ViT-S/16 [5]	$224 \times 224$	81.47	<b>96.20</b>	-	-	22.1M	22.1M
	V-MoE-S/16 [36]		81.19	96.07	32	1	95.3M	22.1M
	V-MoGE-S/16		<b>81.50</b>	96.19	32	1	95.3M	22.1M
	SwinV1-T/7 [30]	$224 \times 224$	80.80	<b>95.94</b>	-	-	28.3M	28.3M
	SwinV1-MoE-T/7 [15]		80.81	95.86	32	1	211.3M	28.3M
	SwinV1-MoGE-T/7		<b>81.06</b>	95.92	32	1	211.3M	28.3M

## 4.1 Image Classification

**Setup.** We leverage three commonly used datasets: CIFAR-100 [24], Tiny-ImageNet [25], and ImageNet-1K [37]. For CIFAR-100 and Tiny-ImageNet, we apply data augmentation techniques as described in [26], while adhering to standard practices [29–31, 46] for ImageNet-1K. We include three widely recognized Transformer models for comparison: Vision Transformer (ViT) [5], Swin Transformer V1 (SwinV1) [30], and Swin Transformer V2 (SwinV2) [29].

Consistent with prior studies, the architecture of each expert within the MoE layer is designed to be identical to the feedforward layer it replaces. However, determining the optimal placement of the MoE layer is more of an art than a precise technical process. For the ViT-based MoE models (V-MoE), the MoE layers are positioned in the last two even-numbered blocks, as suggested in [36, 43]. In the case of SwinV1-based and SwinV2-based MoE models, the placement strategy varies depending on the dataset. For CIFAR-100 and Tiny-ImageNet, we adopt the approach from [15], placing MoE layers in alternate layers within the last two stages. For ImageNet-1K, following [43], MoE layers are inserted exclusively into the last block of each of the last two stages for both SwinV1-based and SwinV2-based MoE models. We set the capacity ratio of MoE models to 1.25 for CIFAR-100 and Tiny-ImageNet, and to 4 for ImageNet-1K. Following [15], a resolution of  $192 \times 192$  is used for SwinV2-based models during training on ImageNet-1K. All MoE

layers consist of 32 experts with top-1 routing. We conduct evaluations in both training from scratch (i.e., pretraining) and fine-tuning scenarios. For fine-tuning on ImageNet-1K, MoE models perform sparse upcycling to initialize experts from dense checkpoints pre-trained on ImageNet-22K [23]. During pretraining, all models are run for 150 epochs, and for fine-tuning, they are trained for 30 epochs, as in [29, 30]. We incorporate batch prioritized routing and load balancing losses as in [36]. MoGE extends the MoE by introducing our group sparse regularization, while all other aspects remain unchanged. Specifically, MoGE reshapes the representation  $z \in \mathbb{R}^{32}$  into a 2D matrix  $Z \in \mathbb{R}^{4 \times 8}$  and applies a  $3 \times 3$  Gaussian lowpass filter. For more training details, please refer to Appendix B. **Results.** Table 2 presents the top-1 accuracy (Acc@1) and top-5 accuracy (Acc@5) achieved by various models across different datasets. The larger the value, the better the result, with the best results highlighted in bold. Notably, MoGE consistently outperforms MoE across all datasets in both top-1 and top-5 accuracies. When trained from scratch on ImageNet-1K, MoGE is inferior to its dense counterpart. This finding aligns with existing studies [14, 43, 50], which indicate that MoE models directly duplicated dense models fail to surpass the performance of their dense counterparts on ImageNet-1K. However, these MoE models demonstrate superior performance on ImageNet-22K. Due to the prohibitive computational cost of training from scratch on ImageNet-22K, we instead

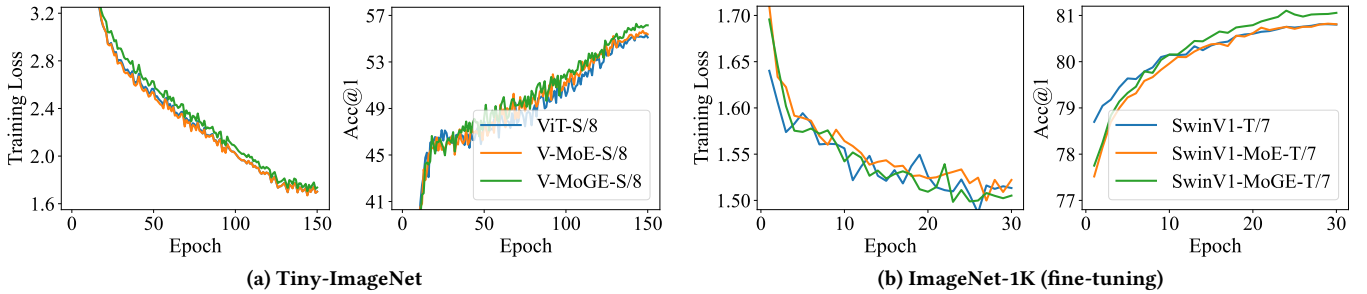


**Figure 4: Training loss and top-1 accuracy curves of dense, MoE, and MoGE models. (a) illustrates training from scratch on Tiny-ImageNet, while (b) showcases fine-tuning on ImageNet-1K.**

fine-tune models that are pretrained on ImageNet-22K. We can see that MoGE achieves better top-1 accuracy than the dense model, while its top-5 accuracy remains comparable.

MoGE and MoE exhibit nearly identical total parameter count (#Params) and active parameter count per token (#Params<sub>act</sub>) across various datasets. Although the total parameters of both MoGE and MoE are substantially larger than those of dense models, their active parameter counts per token remain nearly equivalent. This highlights the advantages of the sparsely activated MoE architecture in scaling up the number of parameters.

Fig. 4 presents parts of the training loss and the top-1 accuracy curves, with additional visualizations provided in Appendix A. Compared to MoE, MoGE incorporates a regularization constraint, which results in its training loss not consistently being lower than that of MoE. However, its top-1 accuracy is significantly higher than that of MoE.

## 4.2 Language Modeling

**Setup.** Following [40], we evaluate the effectiveness of MoGE on WikiText-103 [34] using three types of MoE models: Switch Transformer (SMoE) [7], MomentumSMoE [40], and AdamSMoE [40]. Each MoE layer consists of 16 experts utilizing top-2 routing. MoGE introduces our proposed group sparse regularization to the MoE, while keeping all other aspects unchanged.

For language modeling, the top- $k$  function is typically applied before the softmax function, differing from the sequence introduced in subsection 3.1. Specifically, sparsely activated weights are computed as follows:

$$w = \text{softmax}(\text{TopK}(G(x), k)),$$

where the top- $k$  function,  $\text{TopK}(\cdot, \cdot)$ , is defined as:

$$\text{TopK}(v, k) = \begin{cases} v_i, & \text{if } v_i \text{ is among the top-}k \text{ elements of } v; \\ -\infty, & \text{otherwise.} \end{cases}$$

MoGE can be directly applied to  $G(x)$ . To facilitate tuning of  $\lambda$  in (9), we normalize  $G(x)$  using the softmax function. Thus, we first compute  $z = \text{softmax}(G(x))$  and then pass  $z$  into Algorithm 1 to obtain the group sparse regularization  $R(z)$ . MoGE reshapes  $z \in \mathbb{R}^{16}$  into a 2D matrix  $Z \in \mathbb{R}^{4 \times 4}$  and applies a  $3 \times 3$  Gaussian lowpass filter. For all MoGE models, we set  $\sigma_0 = 10$ ,  $\sigma_{\min} = 1.5$ , and  $\gamma = 0.3$ . For further training details, please refer to Appendix B.

**Table 3: Comparison of the perplexity (PPL) of MoGE across three types of MoE models. The down-arrow notation ( $\downarrow$ ) indicates that a lower value represents better performance.**

Model and Type	$n$	$k$	Valid PPL $\downarrow$	Test PPL $\downarrow$
SMoE-small	16	2	84.26	84.81
SMoGE-small	16	2	<b>82.38</b>	<b>82.08</b>
SMoE-medium	16	2	33.76	35.55
SMoGE-medium	16	2	<b>33.50</b>	<b>35.52</b>
MomentumSMoE-small	16	2	85.71	86.65
MomentumSMoGE-small	16	2	<b>83.10</b>	<b>83.50</b>
MomentumSMoE-medium	16	2	32.29	33.46
MomentumSMoGE-medium	16	2	<b>31.84</b>	<b>33.35</b>
AdamSMoE-medium	16	2	<b>31.69</b>	33.37
AdamSMoGE-medium	16	2	31.86	<b>33.28</b>

**Results.** Table 3 summarizes the perplexity (PPL) values for three types of MoE models on the validation and the test sets of WikiText-103. Lower PPL values indicate better performance, with the best results highlighted in bold. MoGE consistently outperforms MoE across all test sets and most validation sets, clearly demonstrating its superiority. Although MoGE shows slightly inferior performance to MoE on the validation set when using the AdamSMoE-medium model, it still achieves better performance on the more critical test set. Due to space constraints, the training and the validation PPL curves are provided in Appendix A.

## 4.3 Scalability and Efficiency Analysis

**Scaling  $k$  and  $n$ .** We analyze the performance of MoE and MoGE when scaling the number of experts (i.e.,  $n$ ) and the  $k$  value in top- $k$  routing. For this investigation, we use the V-MoE-S/8 and V-MoGE-S/8 models, trained from scratch on Tiny-ImageNet, as in Table 2. The results, summarized in Table 4, consistently demonstrate that MoGE outperforms MoE. Moreover, MoGE exhibits a less significant performance decline as  $n$  and  $k$  increase. This highlights the capacity of MoGE to leverage a higher number of experts and larger  $k$  values, providing substantial evidence for the flexible and scalable design of its experts.

**Table 4: Comparison of MoE and MoGE across different values of  $k$  and  $n$  in image classification.**

Type	$n = 32$				$k = 1$		
	$k=1$	$k=2$	$k=5$	$k=9$	$n=16$	$n=25$	$n=32$
MoE	55.38	53.46	53.58	52.07	55.51	55.22	55.38
MoGE	<b>56.15</b>	<b>53.75</b>	<b>54.17</b>	<b>53.91</b>	<b>55.56</b>	<b>55.46</b>	<b>56.15</b>

**Table 5: Comparison of wall-clock time (WCT, in seconds) and total GPU memory cost (TMC, in MB) between MoE and MoGE.**

Dataset	Model	Type	WCT	TMC
Tiny-ImageNet	ViT-S/8	MoE	40617	5295
		MoGE	40865	5299
	ViT-B/8	MoE	112826	12071
		MoGE	113080	12074
ImageNet-1K (fine-tuning)	SwinV1-T/7	MoE	17343	7163
		MoGE	17554	7167
	SwinV1-B/7	MoE	30791	14547
		MoGE	31017	14549

**Additional Computation and Memory.** Compared to MoE, the additional computational and memory overhead introduced by MoGE primarily depends on the number of experts (i.e.,  $n$ ), rather than the size of the experts or the total parameter count of the MoE model. To empirically validate this fact, we select four models from Table 2 and evaluate them under two scenarios: training from scratch and fine-tuning, with  $n = 32$  and top-1 routing. The results are summarized in Table 5.

The increase in total GPU memory usage for MoGE, compared to MoE, is negligible. When comparing the wall-clock time, we observe that for training ViT-based MoE models from scratch on Tiny-ImageNet, the training time for MoGE increases by no more than 1% compared to MoE. Similarly, for fine-tuning SwinV1-based MoE models on ImageNet-1K, the training time for MoGE increases by no more than 1.5% compared to MoE. Although ViT-S/8 and ViT-B/8 differ significantly in total model parameters, they share the same number of MoE layers, resulting in a comparable absolute increase in training time (248 vs. 254 seconds). Likewise, SwinV-T/7 and SwinV1-B/7 differ in parameter counts but have the same number of MoE layers, leading to a similar absolute increase in fine-tuning time (211 vs. 226 seconds).

#### 4.4 Ablation Study

For our proposed MoGE, we set the hyperparameter  $\lambda$  in Eq. (9) as described in Appendix B. We conduct the following ablation studies for the Gaussian lowpass filter.

**Standard Deviation  $\sigma$ .** We select the SwinV2-MoGE-T/4 model on CIFAR-100 from Table 2 under the scenario of training from scratch, with  $n = 32$  and top-1 routing. With the filter size  $h$  fixed at 3, hyperparameter tuning is performed empirically through the

following steps. First, the optimal  $\sigma$  is identified by conducting a search while keeping  $\sigma$  constant. Next,  $\sigma_0$  is fixed at 10 and  $\sigma_{\min}$  is set to the optimal  $\sigma$  determined in the previous step. The search then focuses on identifying the optimal  $\gamma$ . Finally, using the optimal  $\gamma$  obtained,  $\sigma_{\min}$  is further refined through an additional search. In our experiments, the typical settings are  $h = 3$ ,  $\sigma_0 = 10$ , and  $\gamma = 0.3$ . For each specific task, only  $\sigma_{\min}$  requires tuning.

**Table 6: Ablation study on the Gaussian lowpass filter.**

$\sigma$	Acc@1	$\sigma_0$	$\sigma_{\min}$	$\gamma$	Acc@1	$\sigma_0$	$\sigma_{\min}$	$\gamma$	Acc@1	$h$	Acc@1
3	77.25	2	2	0	77.57	10	2	0.3	77.64	3a	54.90
2.5	77.50	10	2	3.0	77.59	10	1.5	0.3	<b>77.75</b>	3g	<b>55.15</b>
2	<b>77.57</b>	10	2	1.0	77.60	10	1	0.3	77.72	5a	54.31
1.5	77.54	10	2	0.3	<b>77.64</b>	10	0.5	0.3	77.23	5g	54.52

**Filter Size  $h$ .** We select the V-MoGE-S/8 model on Tiny-ImageNet from Table 2 under the scenario of training from scratch. Each MoGE layer consists of 128 experts with top-1 routing, and the corresponding 2D matrix is  $Z \in \mathbb{R}^{8 \times 16}$ . For the average and Gaussian filters, we set  $\lambda = 4e-3$  and evaluate the performance across different values of filter size  $h$ . For the Gaussian filter, we further set  $\sigma_0 = 10$ ,  $\sigma_{\min} = 1.5$ , and  $\gamma = 0.3$ . The results are summarized in the last two columns of Table 6, where “3a” and “5a” represent average filters with sizes  $3 \times 3$  and  $5 \times 5$ , respectively, while “3g” and “5g” denote Gaussian filters with the same respective sizes. From the results, it is evident that filters with  $h = 3$  outperform those with  $h = 5$ , and Gaussian filters consistently achieve better performance compared to average filters.

## 5 Conclusion

This paper introduces a novel perspective on MoE with the widely used top- $k$  routing, grounded in sparse representation. It proposes applying a group sparse regularization to the routing input, referred to as Mixture of Group Experts (MoGE), indirectly imposes structural constraints on the experts. MoGE further organizes the routing input into a 2D topographic map, grouping neighboring elements to encourage the learning of invariant representations. Consequently, MoGE fosters greater diversity and specialization among experts. Extensive experiments across various image classification and language modeling tasks demonstrate that the proposed MoGE consistently outperforms vanilla MoE, while incurring only minimal increases in computation and memory overhead. By scaling both the number of experts and the  $k$  value in top- $k$  routing, MoGE offers a simple yet effective solution that enhances the flexibility of expert design in MoE models.

**Limitations.** Our evaluation is currently limited to image classification and language modeling tasks. Due to constrained computational resources, we have not explored larger-scale MoE models with billions of parameters. Designing novel structural constraints in our MoGE framework tailored to specific tasks is a promising direction worth exploring. Additionally, the expert architecture in MoGE models is currently adapted directly from dense Transformer models, leaving the investigation of optimal expert design as an exciting direction for future research.

## References

- [1] Raquel Aoki, Frederick Tung, and Gabriel L Oliveira. 2022. Heterogeneous multi-task learning with expert diversity. *IEEE/ACM Transactions on Computational Biology and Bioinformatics* 19, 6 (2022), 3093–3102.
- [2] Shane Bergsma, Nolan Simran Dey, Gurpreet Gosal, Gavia Gray, Daria Soboleva, and Joel Hestness. 2025. Straight to zero: Why linearly decaying the learning rate to zero works best for LLMs. In *Proceedings of the International Conference on Learning Representations*.
- [3] Róbert Csordás, Piotr Piękos, Kazuki Irie, and Jürgen Schmidhuber. 2024. Switch-head: Accelerating Transformers with mixture-of-experts attention. *Advances in Neural Information Processing Systems* 37 (2024), 74411–74438.
- [4] David L Donoho and Michael Elad. 2003. Optimally sparse representation in general (nonorthogonal) dictionaries via  $l_1$  minimization. *Proceedings of the National Academy of Sciences* 100, 5 (2003), 2197–2202.
- [5] Alexey Dosovitskiy, Lucas Beyer, Alexander Kolesnikov, Dirk Weissenborn, Xiaohua Zhai, Thomas Unterthiner, Mostafa Dehghani, Matthias Minderer, G Heigold, S Gelly, et al. 2020. An image is worth 16x16 words: Transformers for image recognition at scale. In *Proceedings of the International Conference on Learning Representations*.
- [6] Yonina C Eldar, Patrick Kuppinger, and Helmut Bölcskei. 2010. Block-sparse signals: Uncertainty relations and efficient recovery. *IEEE Transactions on Signal Processing* 58, 6 (2010), 3042–3054.
- [7] William Fedus, Barret Zoph, and Noam Shazeer. 2022. Switch Transformers: Scaling to trillion parameter models with simple and efficient sparsity. *Journal of Machine Learning Research* 23, 120 (2022), 1–39.
- [8] Jinyuan Feng, Zhiqiang Pu, Tianyi Hu, Dongmin Li, Xiaolin Ai, and Huimu Wang. 2025. OMoE: Diversifying mixture of low-rank adaptation by orthogonal finetuning. *arXiv:2501.10062* (2025).
- [9] Yunhao Gou, Zhili Liu, Kai Chen, Lanqing Hong, Hang Xu, Aoxue Li, Dit-Yan Yeung, James T Kwok, and Yu Zhang. 2023. Mixture of cluster-conditional LoRA experts for vision-language instruction tuning. *arXiv:2312.12379* (2023).
- [10] Xumeng Han, Longhui Wei, Zhiyang Dou, Zipeng Wang, Chenhui Qiang, Xin He, Yingfei Sun, Zhenjun Han, and Qi Tian. 2024. ViMoE: An empirical study of designing vision mixture-of-experts. *arXiv:2410.15732* (2024).
- [11] Xu Owen He. 2024. Mixture of a million experts. *arXiv:2407.04153* (2024).
- [12] Ahmed Hendawy, Jan Peters, and Carlo D’Eramo. 2024. Multi-task reinforcement learning with mixture of orthogonal experts. In *Proceedings of the International Conference on Learning Representations*.
- [13] Yaohua Hu, Chong Li, Kaiwen Meng, Jing Qin, and Xiaoqi Yang. 2017. Group sparse optimization via  $l_{p,q}$  regularization. *Journal of Machine Learning Research* 18, 30 (2017), 1–52.
- [14] Yongqi Huang, Peng Ye, Xiaoshui Huang, Sheng Li, Tao Chen, Tong He, and Wanli Ouyang. 2023. Experts weights averaging: A new general training scheme for vision Transformers. *arXiv preprint arXiv:2308.06093* (2023).
- [15] Changho Hwang, Wei Cui, Yifan Xiong, Ziyue Yang, Ze Liu, Han Hu, Zilong Wang, Rafael Salas, Jithin Jose, Prabhat Ram, et al. 2023. Tutel: Adaptive mixture-of-experts at scale. *Proceedings of Machine Learning and Systems* 5 (2023), 269–287.
- [16] Aapo Hyvärinen and Patrik O Hoyer. 2001. A two-layer sparse coding model learns simple and complex cell receptive fields and topography from natural images. *Vision Research* 41, 18 (2001), 2413–2423.
- [17] Aapo Hyvärinen and Urs Köster. 2007. Complex cell pooling and the statistics of natural images. *Network: Computation in Neural Systems* 18, 2 (2007), 81–100.
- [18] Robert A Jacobs, Michael I Jordan, Steven J Nowlan, and Geoffrey E Hinton. 1991. Adaptive mixtures of local experts. *Neural Computation* 3, 1 (1991), 79–87.
- [19] Albert Q Jiang, Alexandre Sablayrolles, Antoine Roux, Arthur Mensch, Blanche Savary, Chris Bamford, Devendra Singh Chaplot, Diego de las Casas, Emma Bou Hanna, Florian Bressand, et al. 2024. Mixtral of experts. *arXiv:2401.04088* (2024).
- [20] Michael I Jordan and Robert A Jacobs. 1994. Hierarchical mixtures of experts and the EM algorithm. *Neural Computation* 6, 2 (1994), 181–214.
- [21] Jared Kaplan, Sam McCandlish, Tom Henighan, Tom B Brown, Benjamin Chess, Rewon Child, Scott Gray, Alec Radford, Jeffrey Wu, and Dario Amodei. 2020. Scaling laws for neural language models. *arXiv:2001.08361* (2020).
- [22] Koray Kavukcuoglu, Marc’Aurelio Ranzato, Rob Fergus, and Yann LeCun. 2009. Learning invariant features through topographic filter maps. In *Proceedings of the IEEE Conference on Computer Vision and Pattern Recognition*. IEEE, 1605–1612.
- [23] Aran Komatsuzaki, Joan Puigcerver, James Lee-Thorp, Carlos Riquelme Ruiz, Basil Mustafa, Joshua Ainslie, Yi Tay, Mostafa Dehghani, and Neil Houlsby. 2023. Sparse Upcycling: Training mixture-of-experts from dense checkpoints. In *Proceedings of the International Conference on Learning Representations*.
- [24] Alex Krizhevsky and Geoffrey Hinton. 2009. Learning multiple layers of features from tiny images. (2009).
- [25] Yann Le and Xuan Yang. 2015. Tiny ImageNet visual recognition challenge. *CS 231N* 7, 7 (2015), 3.
- [26] Seung Hoon Lee, Seunghyun Lee, and Byung Cheol Song. 2021. Vision Transformer for small-size datasets. *arXiv:2112.13492* (2021).
- [27] Dmitry Lepikhin, HyoukJoong Lee, Yuanzhong Xu, Dehao Chen, Orhan Firat, Yanping Huang, Maxim Krikun, Noam Shazeer, and Zhifeng Chen. 2021. GShard: Scaling giant models with conditional computation and automatic sharding. In *Proceedings of International Conference on Learning Representations*.
- [28] Aixin Liu, Bei Feng, Bing Xue, Bingxuan Wang, Bochao Wu, Chengda Lu, Chenggang Zhao, Chengqi Deng, Chenyu Zhang, Chong Ruan, et al. 2024. Deepseek-V3 technical report. *arXiv:2412.19437* (2024).
- [29] Ze Liu, Han Hu, Yutong Lin, Zhuliang Yao, Zhenda Xie, Yixuan Wei, Jia Ning, Yue Cao, Zheng Zhang, Li Dong, et al. 2022. Swin Transformer V2: Scaling up capacity and resolution. In *Proceedings of the IEEE/CVF Conference on Computer Vision and Pattern Recognition*. 12009–12019.
- [30] Ze Liu, Yutong Lin, Yue Cao, Han Hu, Yixuan Wei, Zheng Zhang, Stephen Lin, and Baining Guo. 2021. Swin Transformer: Hierarchical vision Transformer using shifted windows. In *Proceedings of the IEEE/CVF International Conference on Computer Vision*. 10012–10022.
- [31] Zhuang Liu, Hanzi Mao, Chao-Yuan Wu, Christoph Feichtenhofer, Trevor Darrell, and Saining Xie. 2022. A ConvNet for the 2020s. In *Proceedings of the IEEE/CVF Conference on Computer Vision and Pattern Recognition*. 11976–11986.
- [32] Tongxu Luo, Jiahe Lei, Fangyu Lei, Weihao Liu, Shizhu He, Jun Zhao, and Kang Liu. 2024. MoLoRA: Contrastive learning guided mixture of experts on parameter-efficient fine-tuning for large language models. *arXiv:2402.12851* (2024).
- [33] Jiaqi Ma, Zhe Zhao, Xinyang Yi, Jilin Chen, Lichan Hong, and Ed H Chi. 2018. Modeling task relationships in multi-task learning with multi-gate mixture-of-experts. In *Proceedings of the ACM SIGKDD International Conference on Knowledge Discovery & Data Mining*. 1930–1939.
- [34] Stephen Merity, Caiming Xiong, James Bradbury, and Richard Socher. 2017. Pointer sentinel mixture models. In *Proceedings of the International Conference on Learning Representations*.
- [35] Taishi Nakamura, Takuya Akiba, Kazuki Fujii, Yusuke Oda, Rio Yokota, and Jun Suzuki. 2025. Drop-Upcycling: Training sparse mixture of experts with partial re-initialization. In *Proceedings of the International Conference on Learning Representations*.
- [36] Carlos Riquelme, Joan Puigcerver, Basil Mustafa, Maxim Neumann, Rodolphe Jenatton, André Susano Pinto, Daniel Keysers, and Neil Houlsby. 2021. Scaling vision with sparse mixture of experts. *Advances in Neural Information Processing Systems* 34 (2021), 8583–8595.
- [37] Olga Russakovsky, Jia Deng, Hao Su, Jonathan Krause, Sanjeev Satheesh, Sean Ma, Zhiheng Huang, Andrej Karpathy, Aditya Khosla, Michael Bernstein, Alexander C. Berg, and Li Fei-Fei. 2015. ImageNet large scale visual recognition challenge. *International Journal of Computer Vision* 115 (2015), 211–252.
- [38] Noam Shazeer, Azalia Mirhoseini, Krzysztof Maziarz, Andy Davis, Quoc Le, Geoffrey Hinton, and Jeff Dean. 2017. Outrageously large neural networks: The sparsely-gated mixture-of-experts layer. In *Proceedings of International Conference on Learning Representations*.
- [39] Manxi Sun, Wei Liu, Jian Luan, Pengzhi Gao, and Bin Wang. 2024. Mixture of diverse size experts. *arXiv:2409.12210* (2024).
- [40] Rachel S Teo and Tan M Nguyen. 2024. MomentumSMoE: Integrating momentum into sparse mixture of experts. *Advances in Neural Information Processing Systems* 37 (2024), 28965–29000.
- [41] Joel A Tropp. 2004. Greed is good: Algorithmic results for sparse approximation. *IEEE Transactions on Information Theory* 50, 10 (2004), 2231–2242.
- [42] Ashish Vaswani, Noam Shazeer, Niki Parmar, Jakob Uszkoreit, Llion Jones, Aidan N Gomez, Lukasz Kaiser, and Illia Polosukhin. 2017. Attention is all you need. *Advances in Neural Information Processing Systems* 30 (2017).
- [43] Mathurin Videau, Alessandro Leite, Marc Schoenauer, and Olivier Teytaud. 2024. Mixture of experts in image classification: What’s the sweet spot? *arXiv:2411.18322* (2024).
- [44] An Wang, Xingwu Sun, Ruobing Xie, Shuaipeng Li, Jiaqi Zhu, Zhen Yang, Pinxue Zhao, JN Han, Zhanhui Kang, Di Wang, et al. 2024. HMoE: Heterogeneous mixture of experts for language modeling. *arXiv:2408.10681* (2024).
- [45] Liwei Wang, Yan Zhang, and Jufu Feng. 2005. On the Euclidean distance of images. *IEEE Transactions on Pattern Analysis and Machine Intelligence* 27, 8 (2005), 1334–1339.
- [46] Wenhui Wang, Enze Xie, Xiang Li, Deng-Ping Fan, Kaitao Song, Ding Liang, Tong Lu, Ping Luo, and Ling Shao. 2021. Pyramid vision Transformer: A versatile backbone for dense prediction without convolutions. In *Proceedings of the IEEE/CVF International Conference on Computer Vision*. 568–578.
- [47] Danny Wood, Tingting Mu, Andrew M Webb, Henry WJ Reeve, Mikel Lujan, and Gavin Brown. 2023. A unified theory of diversity in ensemble learning. *Journal of Machine Learning Research* 24, 359 (2023), 1–49.
- [48] John Wright, Yi Ma, Julien Mairal, Guillermo Sapiro, Thomas S Huang, and Shuicheng Yan. 2010. Sparse representation for computer vision and pattern recognition. *Proc. IEEE* 98, 6 (2010), 1031–1044.
- [49] Han Xiao, Kashif Rasul, and Roland Vollgraf. 2017. Fashion-MNIST: a novel image dataset for benchmarking machine learning algorithms. *arXiv:1708.07747* (2017).
- [50] Fuzhao Xue, Ziji Shi, Futao Wei, Yuxuan Lou, Yong Liu, and Yang You. 2022. Go wider instead of deeper. In *Proceedings of the AAAI Conference on Artificial Intelligence*.

*Intelligence*, Vol. 36. 8779–8787.

- [51] An Yang, Baosong Yang, Beichen Zhang, Binyuan Hui, Bo Zheng, Bowen Yu, Chengyuan Li, Dayiheng Liu, Fei Huang, Haoran Wei, et al. 2024. Qwen2.5 technical report. *arXiv:2412.15115* (2024).
- [52] Yuqi Yang, Peng-Tao Jiang, Qibin Hou, Hao Zhang, Jinwei Chen, and Bo Li. 2024. Multi-task dense prediction via mixture of low-rank experts. In *Proceedings of the IEEE/CVF conference on computer vision and pattern recognition*. 27927–27937.
- [53] Ming Yuan and Yi Lin. 2006. Model selection and estimation in regression with grouped variables. *Journal of the Royal Statistical Society Series B: Statistical Methodology* 68, 1 (2006), 49–67.
- [54] Yanqi Zhou, Tao Lei, Hanxiao Liu, Nan Du, Yanping Huang, Vincent Zhao, Andrew M Dai, Quoc V Le, James Laudon, et al. 2022. Mixture-of-experts with expert choice routing. *Advances in Neural Information Processing Systems* 35 (2022), 7103–7114.
- [55] Xingkui Zhu, Yiran Guan, Dingkang Liang, Yuchao Chen, Yuliang Liu, and Xiang Bai. 2024. MoE Jetpack: From dense checkpoints to adaptive mixture of experts for vision tasks. *Advances in Neural Information Processing Systems* 37 (2024), 12094–12118.